Jararr *et al. Beni-Suef Univ J Basic Appl Sci* (2025) 14:106
https://doi.org/10.1186/s43088-025-00696-w

Beni-Suef University Journal of Basic and Applied Sciences

RESEARCH

Open Access

Comparative neurobehavioral and histopathological toxicity induced by chronic exposure to metallic oxide nanoparticles and perovskite nanomembrane

Bashir Jararr[1*], Mansour Almansour[2], Amin Al-Doaiss[3], Qais Jarrar[4], Edi Syams Zainudin[5], Su-Jun Lee[6] and Amal Sewelam[7]

Abstract

Background Nanoparticles (NPs) are increasingly used in medicine, industry, agriculture, cosmetics, drug delivery, and energy storage. Despite their widespread use, their potential toxicity, particularly their effects on behavior, remains poorly understood. This study aimed to investigate behavioral and neuronal changes following chronic exposure to four types of NPs: silicon dioxide, nickel oxide, cobalt oxide, and perovskite nanomembrane.

Methods Eighty adult male BALB/c mice were divided into four treatment groups and four control groups. Treated mice received daily intraperitoneal injections of silicon dioxide, nickel oxide, cobalt oxide, or perovskite for 35 days, while controls received the corresponding vehicle. All mice underwent eight neurobehavioral tests. Brain tissues were collected for histological and immunohistochemical analysis.

Results NPs-exposed mice exhibited anxiety- and depression-like behaviors, increased stress, thigmotaxis, reduced locomotion, and impaired exploratory activity. Spatial learning and both reference and working memory were also compromised. Histological analysis revealed neuronal shrinkage and pyknosis in the prefrontal cortex, hippocampus, and cerebellum, along with gliosis, vascular changes, perivascular edema, neuronophagia, and spongiosis. Moreover, a positive inducible nitric oxide synthase (iNOS) immunoreactivity has been increased by the exposure to different types of NPs indicating nitrosative stress with subsequent oxidative stress.

Conclusions Chronic exposure to NPs induces nitrosative and subsequent oxidative stresses-related neuronal damage and behavioral alterations, potentially disrupting brain function. Among the tested NPs, perovskite nanomembranes displayed the most severe effects, followed by Co_3O_4, NiO, and SiO_2 NPs. Further studies are needed to elucidate the relationship between behavioral outcomes and neuronal pathology caused by long-term NP exposure.

Keywords Silicon dioxide NPs, Nickel oxide NPs, Cobalt oxide NPs, Perovskite nanomembrane, Brain, Nanotoxicity

*Correspondence:
Bashir Jararr
bashirjarrar@yahoo.com
Full list of author information is available at the end of the article

1 Background

Nanoparticles have emerged as transformative tools across various sectors. In therapeutics, they enable targeted drug delivery, improving treatment efficacy while reducing side effects [1]. In diagnostics and medical imaging, their unique properties enhance contrast and precision [2]. Industrial applications include catalysis and sensing, contributing to more efficient processes and advanced materials development [3]. In agriculture, NPs support nano-fertilizers, pest control, and precision farming [4]. The food packaging industry uses them to extend shelf life, prevent microbial contamination, and monitor food quality [5]. In cosmetics, NPs improve formulation performance, enabling better skin penetration and sustained release of active ingredients [6]. Perovskite solar cells, a promising renewable energy source, demonstrate power conversion efficiencies of up to 25%, offering high performance and low production costs [7].

Despite this broad utility, the potential toxicity of NPs remains underexplored. Humans may be exposed through inhalation, skin contact, or ingestion, raising health concerns. NPs can penetrate cells and interact with macromolecules and organelles. Studies have shown that they can impair the function of vital organs, including the liver, kidneys, testes, heart, and brain [8, 9]. In particular, their accumulation in the brain has been linked to structural and functional damage [10].

Evidences indicate specific concerns regarding the toxicological profiles of the NPs under investigation. Silicon dioxide NPs have been reported to accumulate in the neuronal tissues, induce oxidative stress, inflammatory responses, and potential genotoxic effects [8]. They are also capable of crossing the blood–brain barrier (BBB), where they can trigger oxidative stress, neuroinflammation, and neuronal apoptosis, potentially impairing cognitive function. Nickel oxide NPs are associated with oxidative and nitrosative stress, cognitive decline, DNA damage, apoptosis, and inflammatory cascades, which may contribute to neurotoxicity outcomes [10]. They may also disrupt neurotransmitter levels and induce neurodegeneration through oxidative damage and inflammation in brain tissues. Cobalt oxide NPs have been shown to cause mitochondrial dysfunction in neural cells and generate reactive oxygen species (ROS), leading to neurotoxicity, cellular damage, and neuronal cell death [9]. Furthermore, lead-based perovskite nanomaterials may release toxic ions, such as lead or halide compounds, posing significant risks to both neuronal and systemic health [7]. Exposure to these materials has been linked to impaired synaptic function and neurodevelopmental alterations.

These impacts underscore the need for more targeted neurotoxicological studies of these NPs, particularly under conditions of chronic exposure, to better understand their impact on brain structure and function. In addition, evidence from multiple studies, including our own, suggests that the brain is particularly vulnerable to NP-induced toxicity [11]. Therefore, the present study aims to assess behavioral and neuronal histological changes following chronic exposure to four types of NPs: silicon dioxide, nickel oxide, cobalt oxide, and perovskite nanomembranes.

2 Materials and methods

2.1 Nanoparticles

2.1.1 Silicon dioxide NPs

Nano-powder of SiO_2 NPs (CAS number 7631-86-9, product number 637246, 15 nm, 99.5% purity, surface area 640 m^2/g) was purchased from Sigma-Aldrich (USA). The nano-suspension was prepared using normal saline as the vehicle. Silicon dioxide NPs were administered intraperitoneally (IP) at a daily dose of 2 mg/kg body weight (bw) for 35 days, while mice in the control group each received an IP injection of 0.2 mL fresh sterilized physiological saline solution as a vehicle [11].

2.1.2 Nickel oxide NPs

Powdered NiO NPs (CAS number 1313-99-1, product number 637130, < 50 nm particle size, density 6.67 ng/mL at 25 °C, bulk density 0.51 g/mL) were purchased from Sigma-Aldrich. A suspension of NiO NPs was prepared in normal physiological saline and administered IP at a dose of 25 mg/kg bw/day for 35 days, while IP injection of 0.2 mL fresh sterilized physiological saline solution as a vehicle was administered to control mice [12].

2.1.3 Cobalt oxide NPs

Porous, spherical, uncoated Co_3O_4 NPs powder of high purity (CAS number 1308-06-1, product number 637025, < 50 nm particle size, density 6.11 g/mL at 25 °C) was purchased from Sigma-Aldrich. The suspension was prepared using distilled water. Mice in the control group received an IP injection of 0.25 mL distilled water, while treated mice received 2.0 mg Co_3O_4 NPs/kg bw IP for 35 days [13].

2.1.4 Perovskite nanomembrane

A perovskite solution with the formula $FA_{0.5}MA_{0.5}PbI_3$ was obtained from the Nano Center at Jordan University of Science and Technology. The perovskite was characterized using the following methods: Particle size was measured using Zetasizer dynamic light scattering, optical characteristics were evaluated using a Cary 5000 UV–VIS–NIR spectrophotometer (300–900 nm), and Fourier Transform Infrared Spectroscopy (FTIR) was conducted over a wavenumber range of 5000–500 cm^{-1}.

All nanoparticle stock suspensions were sonicated for 15 min using an ultrasonic bath cleaner. The water in the bath was maintained at 37 °C and was replenished at regular intervals to ensure consistent ultrasonic power delivery. All nanoparticle suspensions were sonicated at 37 °C for 15 min before injection. The final volume administered IP to each mouse was 250 µL.

In the perovskite-treated group, each mouse received a dose of 0.37 mg/kg bw of perovskite nanomembrane via IP injection, while mice of the control group each received a daily IP dose of 0.8 mg/kg of the organic solvent DMF (*N*,*N*-dimethylformamide) as a vehicle [14]

2.2 Animals and housing conditions

Eighty healthy adult male BALB/c mice, weighing 25–28 g, were used in the present study. Mice were housed in a temperature-controlled environment (22 ± 2 °C) with 50–60% relative humidity and a 12:12-h light–dark cycle. Standard pellet food and drinking water were provided ad libitum.

2.3 Experimental protocol and tissue sampling

Following acclimatization period, the mice were randomly assigned to four main groups ($n = 20$ per group), each corresponding to one type of nanoparticle (SiO_2, NiO, Co_3O_4, or perovskite). Each group was subdivided into a control subgroup ($n = 10$), which received the vehicle only, and a treated subgroup ($n = 10$), which received the corresponding nanoparticle. Intraperitoneal injections were administered daily for 35 consecutive days. The IP route was deliberately selected as a proof-of-concept and exploratory step to obtain reproducible systemic exposure. IP approach allows early identification of intrinsic systemic toxic effects, target organ including brain, and dose–response relationships, which are essential for hazard identification.

All experimental procedures complied with the NIH Guide for the Care and Use of Laboratory Animals and were approved by the Ethics Committee of the University (Approval No. 3/6/2024/2025). Neurobehavioral testing was initiated 24 h after the final NPs injection and continued for a 10-day period. These tests included elevated plus-maze test, open-field maze test, hole-board test, light–dark box test, forced swimming test, tail suspension test, multiradial maze test, and Morris water-maze test.

Neurobehavioral testing began on day 36, 1 day after the final IP injection, with one test conducted per day. Testing concluded on day 45, and all animals were dissected on day 46 for brain harvesting. Neurobehavioral assessment was effectively managed by our laboratory team, which included eight members. The availability of three complete sets of each behavioral maze test and the use of four strategically positioned digital video cameras allowed for sufficient observation and significantly facilitated the timely and parallel execution of the neurobehavioral assessments. Moreover, we implemented randomization procedures to minimize potential stress carry-over. Specifically, animals were randomly assigned to different test times to reduce systematic bias across individuals.

Upon completion of the behavioral assessments, mice were anesthetized with an IP injection of freshly prepared Xylazine/Ketamine solution1 (10:1 ratio, 80 mg/kg Ketamine and 8 mg/kg Xylazine) in saline and sacrificed on day 46. Brains were then excised, rinsed in ice-cold saline, blotted dry, and fixed in buffered neutral formalin. Each brain was sagittal bisected into right and left hemispheres, and processed for histological and immunohistochemical evaluation.

2.4 Histological, immunohistochemical processing, and morphometry

Formalin-fixed brain tissues were dehydrated using a graded series of ethanol, cleared in xylene, and embedded in paraffin wax. Serial coronal sections (4–5 µm thick) were stained with hematoxylin and eosin (H&E) to assess the general histological features of the prefrontal cortex, hippocampus, and cerebellum [15]. Slides were examined using a light microscope, and images were captured with a digital camera. Furthermore, histopathological alterations were graded in all study groups using a semi-quantitative scoring system with a range of 0–3. Six parameters were evaluated histopathologically and scored as follows: inflammation, vascular congestion, perivascular edema, gliosis, vacuolation/spongiosis, and neuronal degenerative markers (neuronal shrinkage, perineuronal halos, and nuclear pyknosis). 0 denotes absence, 1 mild, 2 moderate, and 3 common. Each mouse's histopathological score varied from 0 to 18, which was determined by averaging the scores of these six parameters for each brain per animal per group. Each group's histopathological scores were determined by averaging the values of all the animals in that group [16, 17]. Two observers who were blinded to the groups assessed the histopathological alterations.

For immunohistochemistry, the streptavidin–biotin–peroxidase technique was employed as described by Torlakovic et al. [18]. The expression of iNOS was evaluated using a rabbit monoclonal anti-iNOS antibody (Abcam, 178,945) to assess of nitrosative and subsequent oxidative stress levels. For morphometric analysis, the area % of iNOS protein expression was assessed. In order to assess iNOS protein expression, the immunoreactive area in five non-overlapping high-power fields (400 × magnification) per brain region for each mouse under study was

measured using FIJI/ImageJ software (Version 1.51; NIH, USA). Thresholding was consistently standardized across all images to guarantee uniformity and reproducibility, following the method described by Sewelam et al. [19].

2.5 Neurobehavioral assessment

All behavioral assays were conducted during the light phase of the circadian cycle, within a dedicated, sound-attenuated testing room under dim illumination (< 50 lx). Each apparatus was thoroughly cleaned with a 70% ethanol solution and allowed to dry completely between trials to remove olfactory cues.

To avoid potential stress carry-over between tests, animals were randomized, and test order was counterbalanced across groups, in an attempt to reduce potential confounding.

2.5.1 Elevated plus-maze test

This test aimed to assess anxiety in rodents. This maze is plus shape consists of four arms surround a small central platform (5 cm×5 cm). Two opposing arms are surrounded by high walls (30 cm L×5 cm W×15 cm H) while the others are open (30 cm L×5 cm W). The animal begins on the central platform, facing one of the open arms, and is given 10 minutes to explore the maze. Time spent in each arm, in the central platform, and the number of entrances into closed and open arms were all recorded. An entry was defined as all four paws crossing into the arm.

Typically, animals make significantly more entries into the closed arms. In anxiety-like states, the number of entries into open and closed arms becomes more balanced, and animals are more reluctant to explore the open arms [20]. Additionally, the anxiety index induced by the NPs was calculated in the following formula according to Kraeuter et al. [21]:

$$\text{Anxiety index} = \frac{(\text{closed arm entrances} \times 100)}{(\text{closed arm enterances} + \text{open arm enterances})}$$

2.5.2 The light–dark box maze test

It is designed to test anxiety-like behavior in rodents. Light and new surroundings serve as minor stresses for the rodents. It is made out of a box (45 cm L×27 cm W×27 cm H) with two-thirds of it intended to be an open light chamber and one-third as a covered dark chamber.

Both the chambers are connected with a door (7.5 cm×7.5 cm). The number of transitions between the two chambers and the time spent in each one is recorded. Entry is defined as mouse's four paws are in the chamber [22]. The anxiety index was calculated using the following formula in accordance with Brown and Hascoet [23].

$$\text{Anxiety index} = \frac{(\text{Time spent in the covered dark chamber} \times 100)}{(\text{Time spent in the covered dark chamber} + \text{Time spent in the open light chamber})}$$

2.5.3 Hole-board test

This test evaluates animal's emotionality, neophilia, stress, and anxiety. The device consisted of a 50×50×40 cm Perspex box with 16 holes, 2.5 cm in diameter, drilled through the floor. Exploratory behaviors including thigmotaxis, locomotion, head-dipping, rearing, and central area visiting were observed in each mouse. For 10 min, each animal was placed separately in the middle of the board, and these actions were recorded. To quantify stress-like behavior relative to exploration, a composite stress index was calculated according to Brown and Nemes using the following formula [24]:

$$\text{Stress index} = \frac{(\text{Thigmotaxis} \times 100)}{(\text{Head dipping} + \text{Rearing} + \text{Center movement})}$$

2.5.4 Tail suspension test

This test is a widely used method for assessing depression-like behavior in rodents by measuring immobility time, mobility time, and related behavioral parameters. For 5 minutes, the animal is suspended by its tail from a tube about 10 cm above the ground. The animal will

attempt to flee and grab for the ground during this moment. It is timed to see how long it stays immobile. It is based on the finding that mice would become immobile when exposed to brief, unavoidable stress. The depression-like behavioral index was calculated based on the following formula according to Can et al. [25]:

$$\text{Depression - index} = \frac{(\text{immobility time} \times 100)}{\text{Total time}(\text{Immobility time} + \text{mobility time})}$$

2.5.5 The forced swimming test

This test was performed to assess depression behavior. Mice were located in a clear cylindrical glass container (30×30×50 cm) filled with water (25 ± 1°C) to a depth that the mouse cannot touch the bottom with its hind legs. Mice were skilled to swim for 15 min. After, 24 h, they were enforced to swim again for 6 min through which the immobility duration was recorded. Key parameters assessed include swimming time, immobility time, the number of swimming events, the average time spent in arrest, and the number of climbing attempts. If the animal was passively floating with just slight movements to maintain its head above the water, it was deemed motionless [26]. The depression index was considered according to Can et al. using the following formula [27]:

$$\text{Depression} - \text{index} = \frac{(\text{immobility time} \times 100)}{(\text{Swimming time} + \text{immobility time})}$$

2.5.6 The multiradial maze test

The purpose of this test was to assess rodents' working memory and reference memory. It consists of central area with eight arms extending from it. The distant end of each arm may contain a prize (food based), designed to be not obvious from the central platform. The mouse is placed on the center of the platform and allowed to explore the arms freely for the reward. Since consumed food is not replaced, the mice should enter each arm only once. Between arm visits, the animal must return to the center, where the same eight options are provided each time. The mouse then has to recall which options have already been selected [28]. Additionally, the working memory index is the average number of entrances to the arm with no food while the reference memory index (RMI) was calculated according to Vorhees and Williams by using the following formula [29]:

$$\text{RMI} = \frac{(\text{Number of entrances to the arm with food}) \times 100}{(\text{Total number of visited arm})}$$

2.5.7 Morris water-maze test

It is composed of a circular tank with dimensions of approximately 110 cm in diameter and 40 cm in height with a platform that permits the mouse to escape the water. The water depth is maintained at 25 cm. Each mouse was located in the pool to discover the obvious platform, and the time taken to locate the platform in each trial was recorded. The following metrics were used to assess the overall activity: the number of climbing attempts, swimming time, immobility time, and escape latency (time to locate the platform) [30].

2.5.8 Marble-burying test

This test is a widely used behavioral assay to assess compulsive and obsessive-like behaviors in rodents, often reflecting underlying neurobehavioral and neurochemical disturbances [31]. The test provides insight into the compulsive–obsessive index (COI) by evaluating the number of marbles buried within a specific timeframe. Mice were individually placed in a standard clean cage (36×20×14 cm) containing a 5-cm deep layer of fresh bedding. Twenty glass marbles (1.5 cm diameter) were arranged in a regular 4×5 grid on the surface of the bedding. Each mouse was left in the cage for 30 min. Afterward, the number of marbles buried (defined as being at least two-thirds covered by bedding) was counted.

The COI was calculated according to Angoa-Pérez et al. from the following formula [32]:

$$\text{COI} = \frac{(\text{Number of marbles unburied at 15 min} + \text{Number of marbles unburied at 30 min}) \times 100}{\text{Maximum number of marbles available}}$$

2.6 Statistical analysis

The data were represented as mean ± standard deviation (SD). The comparison between the groups was done using *ANOVA* followed by Tukey post hoc test for multiple comparison. The assumption of homogeneity of variances was verified using Levene's test. For all significant ANOVA results, the effect size was calculated using eta-squared (η^2). p value was considered significant when its value less than 0.05. All statistical analyses were done using SPSS software (Version 26, USA).

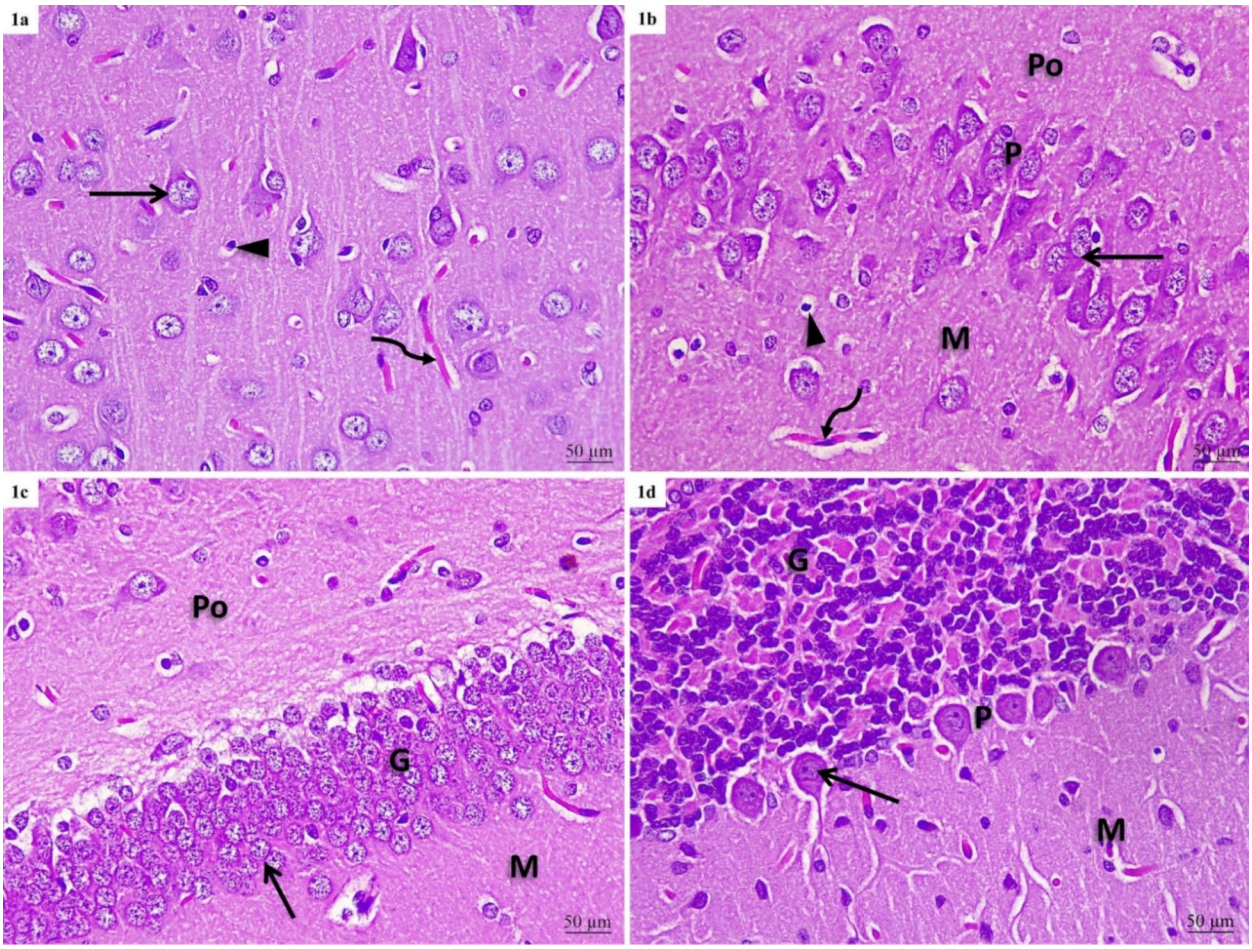

Fig. 1 **a–d** Light H&E-stained micrographs of control brain mice. **a** The inner pyramidal layer of prefrontal cortex presents normal large pyramidal neurons (arrow). **b** Hippocampal CA3 subfield displaying normal molecular (M), pyramidal (P), and polymorphic (Po) layers, **c** hippocampal dentate gyrus with normal molecular (M), granular (G), and polymorphic (Po) layers, and **d** cerebellar cortex with normal granule (G), Purkinje (Pr), and molecular (M) layers. Note normal neurons (arrow), neural capillaries (curved arrow), and glial cells (arrowhead). Scale bar = 50 µm (H&E, × 400)

3 Results

3.1 Histological changes

To standardize the comparison, brain histological and immunohistochemical analysis was performed on each mouse included in the study. The following brain areas were examined: the internal pyramidal layer of the prefrontal cortex, the hippocampus (which included the Cornu Ammonis subfield CA3 and the hippocampal dentate gyrus), and the cerebellar cortex.

3.1.1 Neuronal histological components of the control mice

Brain sections of the four control subgroups exhibited almost similar histological construction. The inner pyramidal layer of prefrontal cortex presented large- and medium-sized pyramidal neuronal cell bodies having large, rounded, vesicular nuclei with prominent nucleoli and basophilic cytoplasm. Also, neuroglia seen as small cells with dark nuclei, blood capillaries, and neuropil (meshwork formed of neuronal and glial processes) were distinguished (Fig. 1a). Regarding CA3 hippocampal subfield, well-defined three layers were displayed: polymorphic layer containing glial cells, pyramidal cell layer exhibiting large pyramidal neurons having large rounded vesicular nuclei, and molecular layer containing mainly the dendrites of the pyramidal neurons (Fig. 1b). In addition, the hippocampal dentate gyrus exhibited three layers: molecular, granular (the principal cell layer being formed of small, rounded neurons), and polymorphic layers (Fig. 1c). Moreover, the cerebellar cortex of control mice exhibited a normal molecular layer, rich in dendrites of normal Purkinje cells layer consisting of a single row of large neurons with large, rounded, pale nuclei and prominent nucleoli. The granular cell layer appeared densely packed with small granule cells, alongside Purkinje and Golgi cells (Fig. 1d).

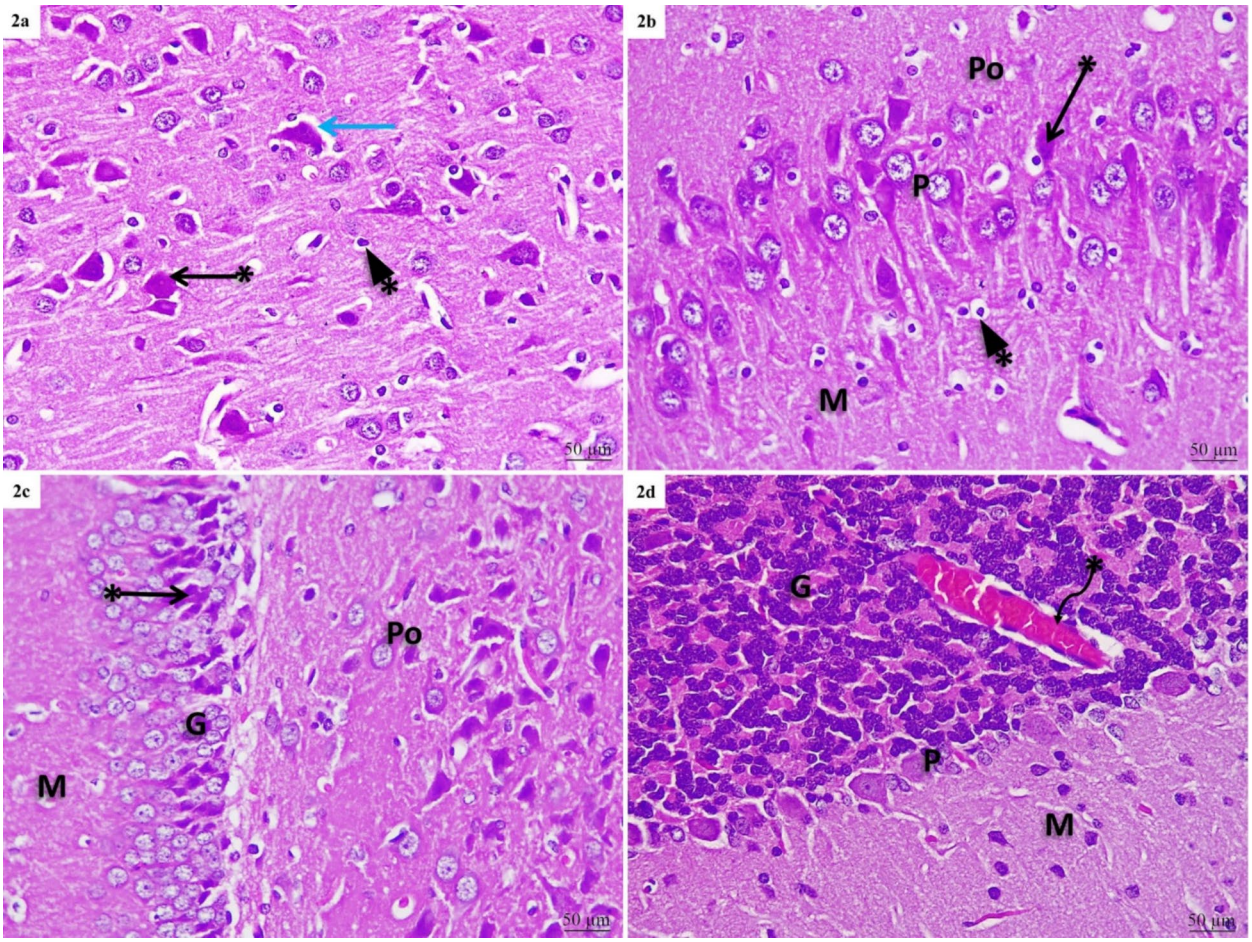

Fig. 2 **a–d** Light H&E-stained micrographs of mice exposed to SiO_2 NPs. **a** Prefrontal cortex, **b** CA3 hippocampal subfield, **c** dendate gyrus, and **d** cerebellar cortex. Note, shrunken neurons with pyknotic nuclei and perineuronal spacing (arrow*), gliosis (arrowhead*), neurophagia (blue arrow), and vascular congestion with perivascular edema (curved arrow*). In addition, molecular (M), pyramidal (P), polymorphic (Po), granular (G), and Purkinje (Pr) layers are obvious. Scale bar = 50 µm (H&E, × 400)

3.1.2 Neuronal histological alterations induced by NPs treatment mice

Histological analysis of the prefrontal cortex, hippocampal CA3 subfield, dentate gyrus, and the cerebellar cortex of all mice under study subgroups exposed to NPs treatment revealed the following significant histological alterations.

3.1.2.1 Neuronal histological alterations induced by SiO_2 NPs The prefrontal cortex of this group of NPs-treated mice exhibited shrunken neurons with pyknotic nuclei, perineuronal spacing, gliosis, and neuronophagia (Fig. 2a). The hippocampal CA3 subfield showed gliosis associated with occasional pyramidal neuronal pyknosis (Fig. 2b) and a similar granular neuronal pyknosis in the dentate gyrus (Fig. 2c). However, apart from vascular congestion and perivascular edema in the granule cell layer, the cerebellar cortex remained largely unaffected (Fig. 2d).

3.1.2.2 Neuronal histological alterations induced by NiO NPs Mice exposed to NiO NPs showed cortical vascularization and neuronal nuclear pyknosis (Figure 3a). The hippocampal CA3 subfield displayed pyknotic pyramidal neurons with perineuronal spacing (Figure 3b), while the dentate gyrus exhibited occasional pyknotic granular neurons associated with vascular congestion and perivascular edema (Figure 3c). The cerebellar cortex of these mice showed marked vascular congestion associated with Purkinje cell shrinkage and nuclear pyknosis (Figure 3d).

3.1.2.3 Neuronal histological alterations induced by Co_3O_4 NPs Mice treated with Co_3O_4 NPs showed shrunken pyknotic neurons in the prefrontal cortex, along with vascular congestion and perivascular edema (Fig. 4a). In the hippocampus, the CA3 subfield exhibited extensively shrunken pyknotic pyramidal neurons with perineuronal spacing (Fig. 4b), and the dentate

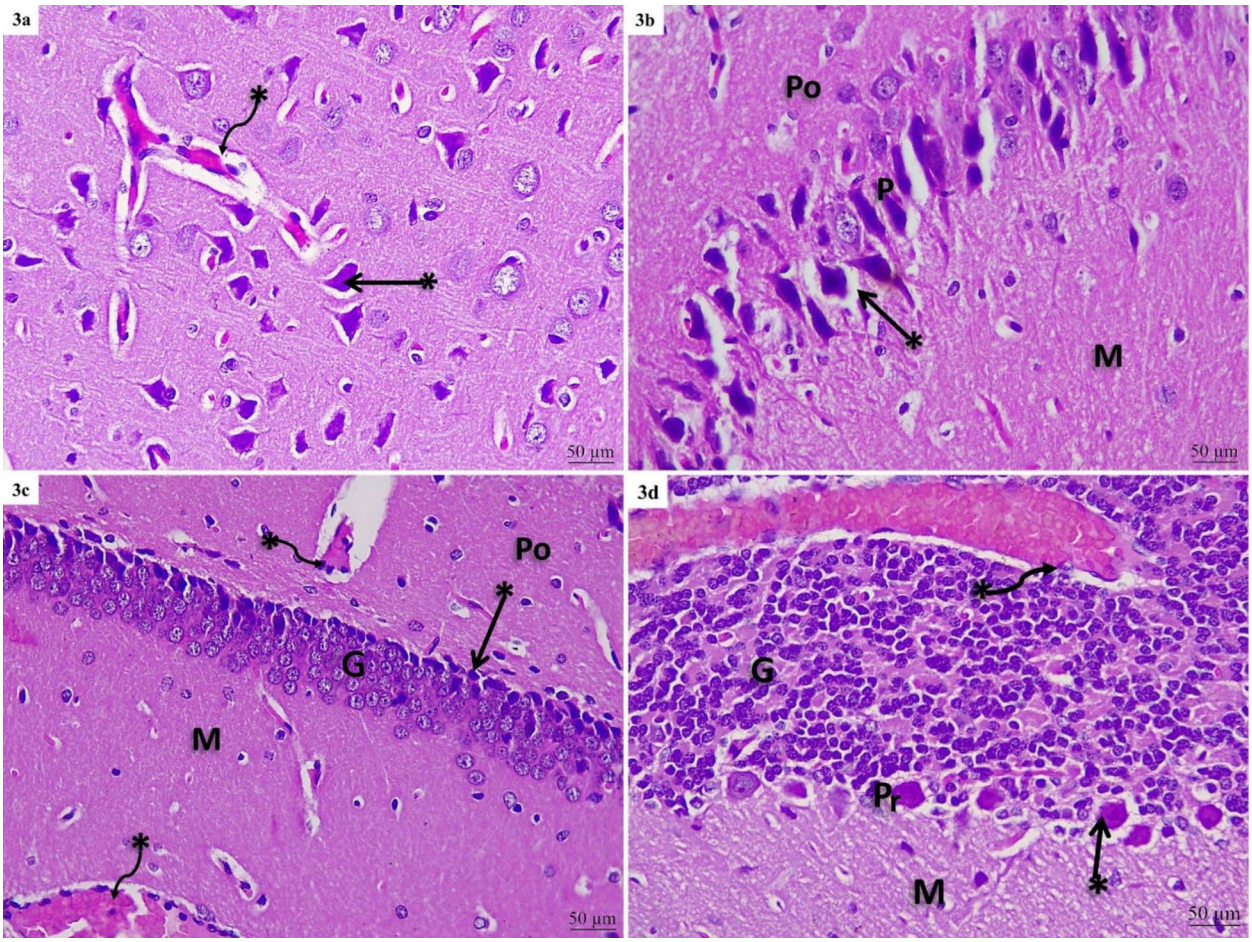

Fig. 3 **a–d** Light H&E-stained micrographs of mice treated with NiO NPs. **a** Prefrontal cortex, **b** CA3 hippocampal subfield, **c** dendate gyrus, and **d** cerebellar cortex. Note, shrunken neurons with pyknotic nuclei and perineuronal spacing (arrow*), vascular congestion with perivascular edema (curved arrow*). In addition, molecular (M), pyramidal (P), polymorphic (Po), granular (G), and Purkinje (Pr) layers are distinguished. Scale bar = 50 µm (H&E, × 400)

gyrus showed shrunken, pyknotic granular neurons (Fig. 4c). The cerebellar cortex displayed Purkinje cell pyknosis, extensive vascular congestion, and neuropil vacuolation (Fig. 4d).

3.1.2.4 Neuronal histological alterations induced by perovskite nanomembrane In mice exposed to perovskite nanomembrane, severe neuronal injury and neurodegeneration were exhibited. The prefrontal cortex (Fig. 5a), hippocampal CA3 subfield (Fig. 5b), dentate gyrus (Fig. 5c), and cerebellar cortex (Fig. 5d) exhibited variable degrees of neuronal damage including shrinkage with pyknosis, chromatolysis, neuronophagia, and necrosis. In addition, neural spongiosis and edema, diffuse gliosis, astrocyte hypertrophy, and neuropil vacuolation were also demonstrated. Further, focal gliosis (Fig. 5e) and congested choroid plexus vasculature (Fig. 5f) were displayed.

3.1.2.5 Histopathological scoring As presented in Table 1, the histopathological brain damage scoring increased with a varying degree in the four NPs-treated groups relative to control group. Post hoc Tukey's HSD analysis showed a statistically significant in total histopathological damage, as following: perovskite NPs > Co_3O_4 NPs > NiO NPs > SiO_2 NPs ($p < 0.05$ for all sequential pairwise comparisons).

3.1.3 Immunohistochemical alterations

The positive iNOS immune reaction appeared as brown coloration in the brain tissue sections. Brain sections of the four control subgroups exhibited almost similar immunohistochemical reaction that appeared non-specific or minimally positive (Fig. 6a–d). Nevertheless, a varying degree of iNOS immune positive reactivity was distinguished in all NPs-treated groups. The immune reaction was apparently mild

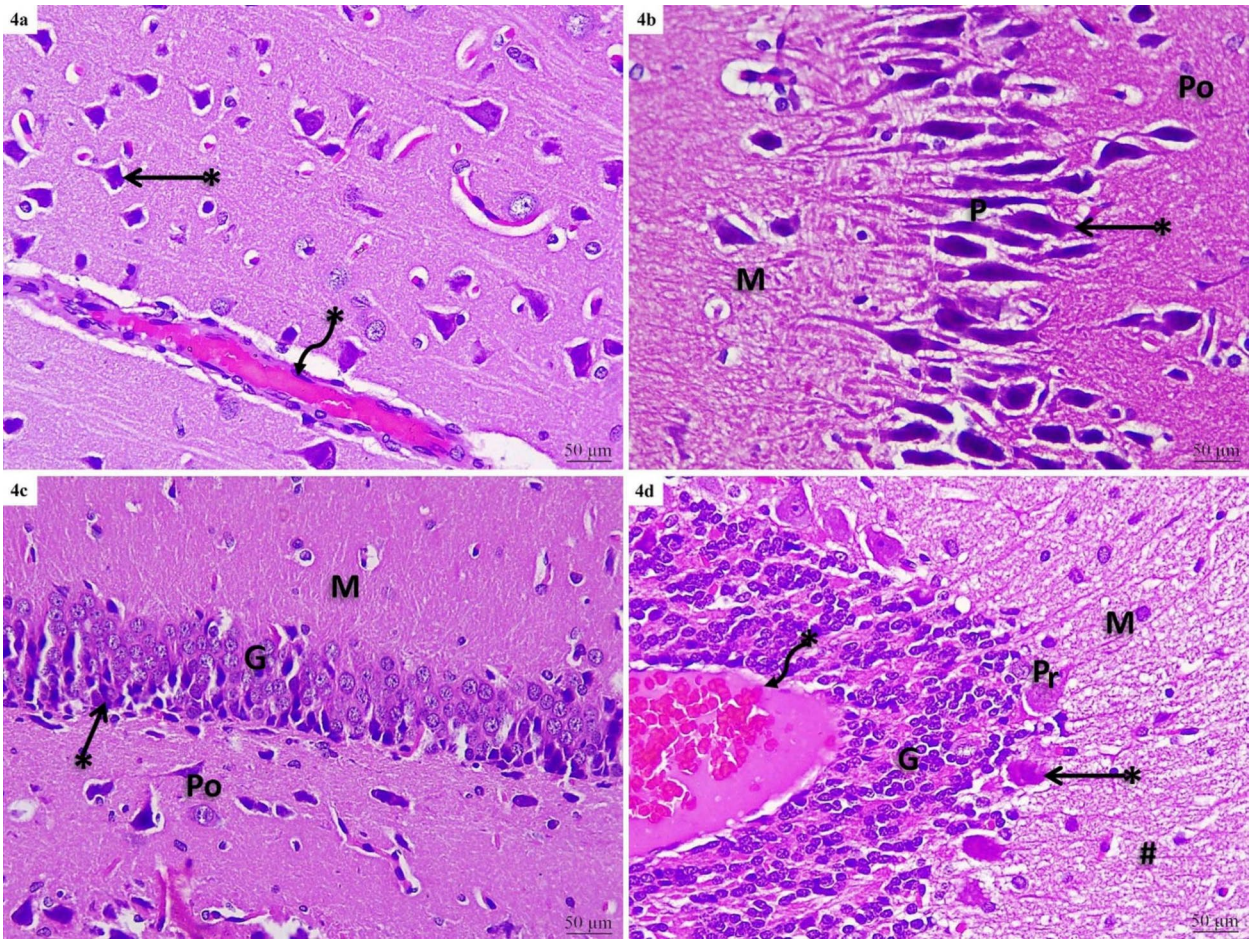

Fig. 4 **a–d** Light H&E-stained micrographs of mice treated with Co_3O_4 NPs. **a** Prefrontal cortex, **b** CA3 hippocampal subfield, **c** dendate gyrus, and **d** cerebellar cortex. Note, shrunken neurons with pyknotic nuclei and perineuronal spacing (arrow*), vascular congestion with perivascular edema (curved arrow*), vacuolated neuropil (#). Also, molecular (M), pyramidal (P), polymorphic (Po), granular (G), and Purkinje (Pr) layers are obvious. Scale bar = 50 µm (H&E, × 400)

positive in SiO_2 NPs-treated mice (Fig. 6e–h), moderately positive in both NiO NPs (Fig. 6i–l) and Co_3O_4 NPs (Fig. 6m–p) treated mice, but strongly positive in perovskite nanomembrane-treated mice (Fig. 6q–t). These observations were confirmed by morphometry findings. The mean values of area percentage (area %) of iNOS expression have been shown a significant difference ($p < 0.05$) regarding the prefrontal cortex, hippocampal CA3 subfield, dentate gyrus, and cerebellar cortex in all groups under study (Table 2). The current study suggested that the positive iNOS immune reactivity has been increased by the exposure to different types of NPs indicating a variable degree of nitrosative stress with subsequent oxidative stress. In comparison between the administrated NPs, statistical analysis using Tukey's HSD test showed a significant stepwise increase in iNOS expression across the treatment groups for all brain regions examined, in a following order: perovskite NPs > Co_3O_4 NPs > NiO NPs > SiO_2 NPs, as presented in Table 2.

3.2 Behavioral alterations

Compared to the control mice in each group, the NPs under investigation exhibited the following distinct behavioral alterations:

3.2.1 Anxiety induction

3.2.1.1 The elevated plus-maze test Compared with the control mice, the treated mice with SiO_2 NPs displayed mild anxiety, while Co_3O_4 NPs produced significant neurobehavioral effects (Table 3). In contrast, NiO NPs and the perovskite nanomembrane showed a high anxiety index.

3.2.1.2 The light–dark box maze test The light–dark box maze is a widely used neurobehavioral test to assess

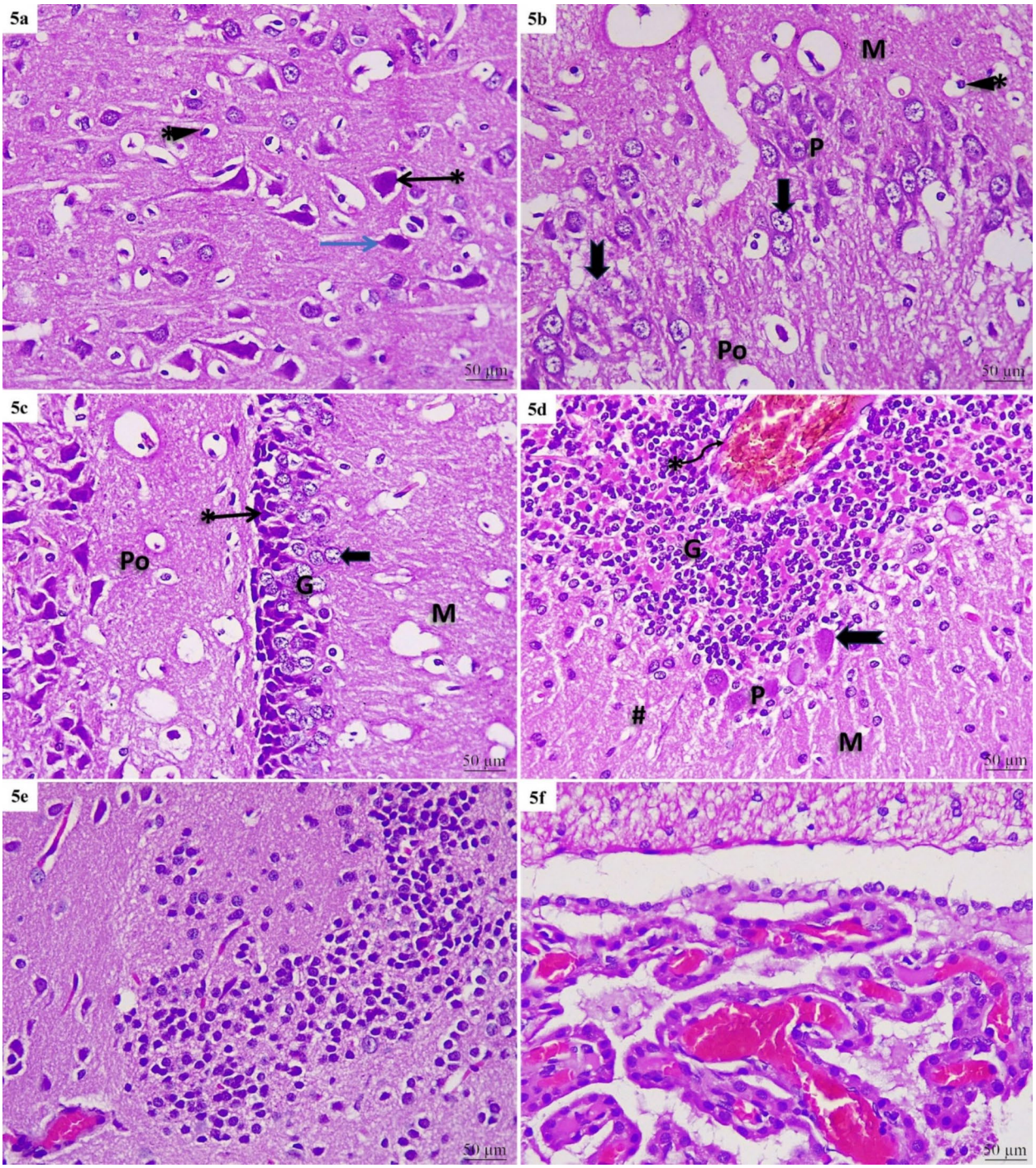

Fig. 5 **a–f** Light H&E-stained micrographs of perovskite NPs-exposed mice. **a** Prefrontal cortex, **b** CA3 hippocampal subfield, **c** dendate gyrus, **d** cerebellar cortex, **e** focal gliosis, and **f** congested choroid vasculature. Note, diffuse gliosis with hypertrophied astrocytes (arrowhead*), neuronal shrinkage with pyknosis (arrow*), neuronophagia (blue arrow), neuronal necrosis (notched arrow), chromatolysis (thick arrow), vascular congestion (curved arrow*), vacuolated neuropil (#), spongiosis, and edema. Further, molecular (M), pyramidal (P), polymorphic (Po), granular (G), and Purkinje (Pr) layers are visible. Scale bar = 50 µm (H&E, × 400)

Table 1 The average distribution of histopathological scores among the various study groups

Histopathology	Group Control	SiO_2 NPs	NiO NPs	CO_3O_4 NPs	Perovskite NPs
Neuronal degeneration	0.25	1.55	2.2	2.8	3
Vascular congestion	0	1.2	1.8	2.8	3
Perivascular edema	0	1.45	1.8	2.2	2.8
Gliosis	0.25	2.8	2.2	1.8	2.8
Vacuolation/Spongiosis	0	1.2	1.2	2.4	3
Inflammatory infiltration	0	0	0.8	0	2.6
Total score	0.5	8.2*	10*,□	12*,#	17.2*,†

0–3 (0: absent, 1: mild, 2: moderate, and 3: common). The score for each mouse ranged from 0 to 18. "*" indicates statistical difference using post hoc Tukey test in comparison with the control group, "□" indicates statistical significance between NiO vs. SiO_2 NPs, "#" indicates statistical significance between Co_3O_4 vs. NiO NPs, and "†" indicates statistical significance between perovskite vs. Co_4O_4 NP, p value < 0.05 is significant

anxiety-like behaviors in rodents. In comparison with control mice, exploratory investigating activities (transitions between the light and dark chambers, partial entries, peeking, or sniffing at the door), all NPs-treated mice demonstrated a significant increase in anxiety levels and variability in the time taken to locate the maze door. Additionally, apart from the SiO_2 NP- and NiO NP-treated groups, a significant increase in anxiety levels was demonstrated in all other NP-treated mice (Table 4).

3.2.2 Stress induction

3.2.2.1 The hole-board test This test is a widely used method for assessing exploratory behavior and stress responses in rodents. As shown in Table 5, the test results reveal significant variations in neurobehavioral parameters between the control and NPs-treated groups.

Control mice frequently exhibited rearing behavior, whereas NPs-treated mice showed significant reductions in this activity, reflecting impaired motor function and heightened stress consistent with neurobehavioral inhibition. Furthermore, center exploration, inversely correlated with anxiety and stress, was markedly reduced in NPs-treated groups compared to control animals. Mice with higher anxiety levels tend to avoid the center of the arena. Finally, control mice exhibited the lowest stress index, consistent with normal exploratory behavior. In contrast, all NPs-treated groups showed elevated stress indices, indicating increased stress responses and significant neurobehavioral disruptions.

3.2.3 Depression aggravation

3.2.3.1 Tail suspension test As shown in Table 6, the control mice displayed the highest mobility time, the lowest immobility time, and favorable behavioral indices for escape attempts and rest, indicating normal neurobehavioral activity. In contrast, NPs-treated mice exhibited reduced mobility time, increased immobility time, and a significant rise in the depression-like behavioral index compared to the control group.

3.2.3.2 The forced swimming test The forced swimming test is a widely used neurobehavioral assay to evaluate depressive-like behavior in rodents.

As demonstrated in Table 7, control mice exhibited the longest swimming time, the shortest immobility time, and the lowest depression index compared to all groups treated with NPs, suggesting normal neurobehavioral activity and a low depressive-like phenotype. NPs-treated mice showed variable reductions in swimming time and increased immobility compared to the control mice. In addition, NPs groups demonstrated fewer swimming events (the count of distinct swimming episodes, horizontal movements in the chamber without climbing), longer average arrest times, and more climbing attempts, accompanied by elevated depression indices, indicative of mild to severe depressive-like behavior.

3.2.4 Effects on memory

3.2.4.1 The multiradial maze test As presented in Table 8, significant neurobehavioral differences are among groups treated with NPs-treated mice compared with the control ones. Control mice displayed the highest number of arm visits, indicating intact exploratory behavior, cognitive and prefrontal cortical function. On the other hand, all treated groups showed reduced exploration, with mice treated with perovskite NPs exhibiting the most pronounced decline. This suggests potential impairment in spatial exploration and overall activity, likely due to the neurotoxic effects of the NPs. The observed decrease in arm entries containing food indicates a progressive disruption in reference memory and goal-directed behavior among NP-treated groups. Furthermore, repeated entries into non-food arms suggest varying levels of working

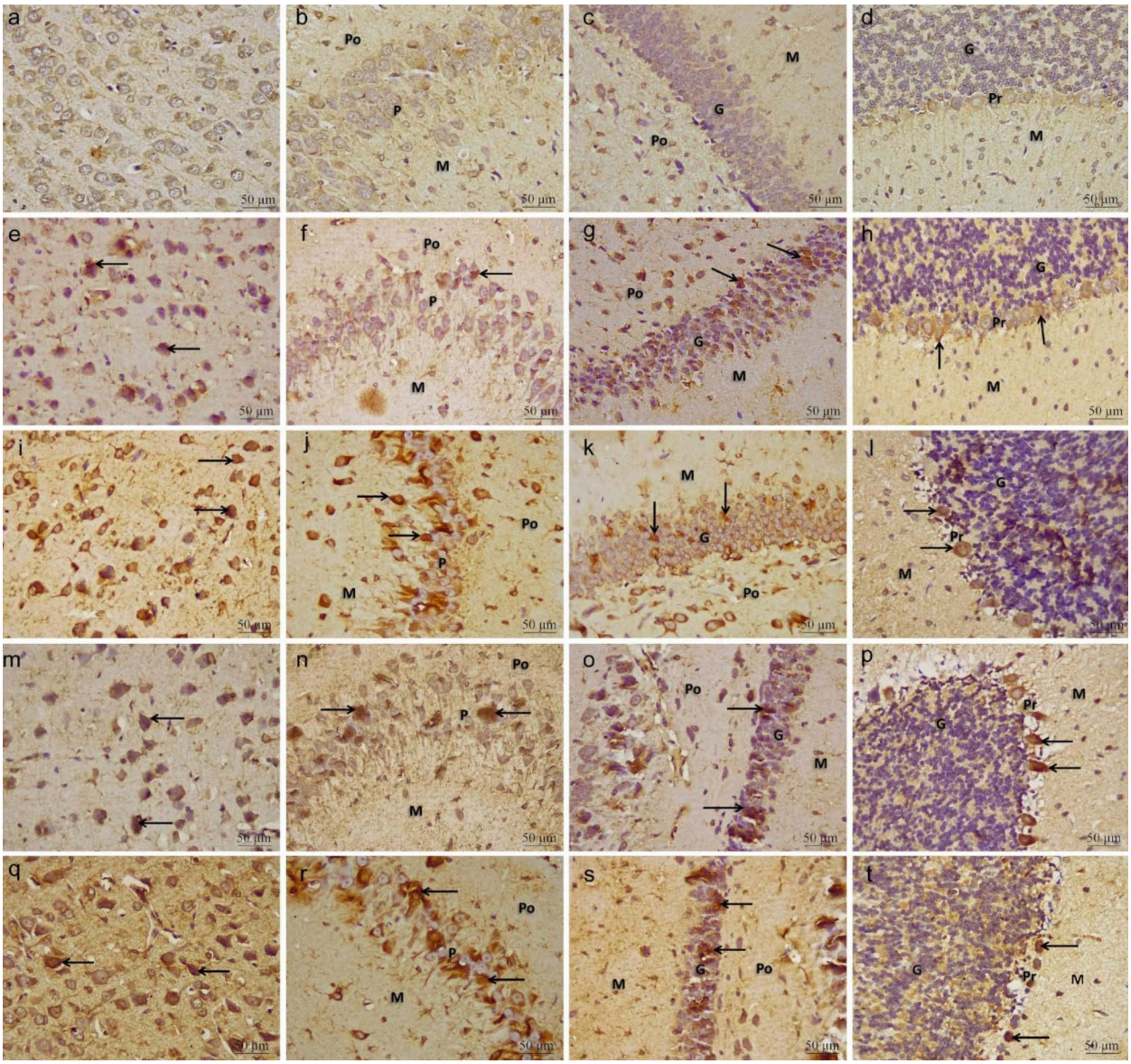

Fig. 6 **a**–**t** Immunohistochemical photographs of brain sections of control (**a**–**d**), SiO_2 NPs (**e**–**h**), NiO NPs (**i**–**l**), Co_3O_4 NPs (**m**–**p**), and perovskite nanomembrane (**q**–**t**) treated mice showing the prefrontal cortex, hippocampal CA3 subfield, hippocampal dentate gyrus, and cerebellar cortex stained with inducible nitric oxide synthase (iNOS) antibody. Black arrows represent the positive areas for the applied antibody. The layers of CA3 subfield are labeled as molecular (M), pyramidal (P), and polymorphic (Po). Also, the layers of dendate gyrus are marked as molecular (M), granular (G), and polymorphic (Po) while those of the cerebellar cortex are presented as molecular (M), Purkinje (Pr), and granular (G). Scale bar = 50 µm (iNOS immunostaining, ×400)

memory impairment, potentially linked to the neurotoxic potential of each nanoparticle type.

3.2.4.2 Morris water-maze test This test is a widely used neurobehavioral assay to evaluate spatial learning and memory in rodents. The escape latency, which measures the time taken to locate the platform, is a critical indicator of spatial learning ability. Control mice exhibited the shortest latency, indicating intact spatial learning and memory. In contrast, a significant increase in escape latency compared to the control group suggests that the NPs under investigation may impair spatial learning (Table 9).

3.2.5 Compulsive disorder induction

3.2.5.1 Marble-burying test This test is considered as an indicator for compulsive disorder among rodents. As shown in Table 10, a decrease in both number of mar-

Table 2 A statistical comparison between different groups regarding the mean area % of iNOS immune reaction in adult mice

Brain region	Group Control	SiO_2 NPs	NiO NPs	CO_3O_4 NPs	Perovskite NPs	*p*	Size effect (η^2)
Prefrontal cortex mean area% ± SD	2.1 ± 0.4	26.2 ± 2.0 *	32.5 ± 4.8*,□	37.2 ± 4.5*, #	45.9 ± 6.2 *,†	< 0.001	0.82
Hippocampal CA3 mean area% ± SD	5.2 ± 0.4	19.8 ± 2.0 *	28.5 ± 4.4*,□	31.2 ± 5.6*,#	35.8 ± 7.0 *,†	< 0.001	
Dendate gyrus mean area% ± SD	3.1 ± 0.5	23.7 ± 1.6 *	19.7 ± 3.6 *,□	34.2 ± 3.6*,#	45.8 ± 4.1*,†	< 0.001	
Cerebellar cortex mean area% ± SD	2.7 ± 0.4	14.6 ± 0.5 *	22.6 ± 2.5*,□	25.2 ± 3.4*,#	29.7 ± 5.1*,†	< 0.001	

p value was calculated using one-way *ANOVA* test. "*" indicates statistical difference using post hoc Tukey

test in comparison with the control group, "□" indicates statistical significance between NiO vs. SiO_2 NPs, "#" indicates statistical significance between Co_3O_4 vs. NiO NPs, and "†" indicates statistical significance between perovskite vs. CO3O4 NP_s. SD = Standard Deviation, *p* value < 0.05 is significant, number of selected mice = 10 for each group, iNOS = inducible nitric oxide synthase

Table 3 The elevated plus-maze test results

Elevated plus-maze test	Average time spent in the center (s)	Average time spent in the open arms (s)	Average time spent in the closed arms (s)	Average # of entries to the open arms	Average # of entries to the closed arms	Average # of end arms exploration	Anxiety index
Control	14 ± 2.1	117 ± 17.5	177 ± 26.6	12.6 ± 1.9	14.7 ± 2.2	4.9 ± 0.7	53.9 ± 8.9
SiO_2 NPs	19 ± 2.9	54 ± 8.1*	411 ± 61.7*	2.3 ± 0.4*	3.2 ± 0.7*	2.2 ± 0.3*	56.1 ± 7.4
NiO NPs	40 ± 6.0*	31 ± 4.7*	548 ± 82.2*	1.7 ± 0.6*	4.7 ± 1.1*	1.9 ± 0.4*	73.4 ± 11.9*
Co_3O_4 NPs	47 ± 7.1*	50 ± 7.5*	512 ± 76.8*	4.5 ± 0.9*	7.7 ± 1.2*	2.3 ± 0.9*	63.1 ± 9.1*
Perovskite NPs	79 ± 11.9*	98 ± 14.7*	351 ± 52.7*	3.8 ± 0.6*	9.7 ± 1.7*	2.1 ± 0.4*	77.0 ± 12.6*
p-value	0.042	0.015	0.009	0.021	0.033	0.044	0.008
Size effect (η^2)	0.48	0.55	0.58	0.51	0.49	0.47	0.60

p value was calculated using one-way *ANOVA* test. "*" indicates statistical difference using post hoc Tukey test in comparison with the control group. η^2 indicates a large effect size

Table 4 The light–dark box maze test results

The dark–light open test	Time spent to find the door (s)	Time spent in the light chamber (s)	Time spent in the dark chamber(s)	Average number of entries to the dark area	Number of exploring	Anxiety index
Control	7.9 ± 1.2	310 ± 46.5	275 ± 41.3	5.1 ± 0.8	11.5 ± 1.7	47.0 ± 7.1
SiO_2 NPs	43.1 ± 8.5*	210 ± 38.5	244 ± 26.6	2.7 ± 0.4	6.8 ± 1.9*	53.7 ± 8.1
NiO NPs	60.5 ± 9.1*	330 ± 49.5	370 ± 65.5*	14.2 ± 2.1*	2.9 ± 0.8*	52.9 ± 7.9
Co_3O_4 NPs	107.7 ± 22.2*	162 ± 31.3*	412 ± 69.8*	15.11 ± 2.3*	2.5 ± 0.5*	71.8 ± 10.8*
Perovskite NPs	98.5 ± 21.8*	322 ± 42.3	475 ± 76.3*	5.1 ± 0.8	2.7 ± 0.4*	59.6 ± 9.9*
p-value	< 0.001	0.021	0.007	0.065	0.012	0.04
Size effect (η^2)	0.78	0.52	0.57	0.38	0.54	0.46

p value was calculated using one-way *ANOVA* test. "*" indicates statistical difference using post hoc Tukey test in comparison with the control group. η^2 indicates a large effect size

bles buried after 15 and 30 min in all NPs-treated groups compared to the control group. The control group buried an average of 6.45 marbles after 15 min and 11.72 marbles after 30 min, resulting in a COI of 1.10. These values serve as the baseline for normal marble-burying behavior indicating minimal compulsive–obsessive tendency. As shown in Table 10, all NPs-treated mice buried fewer marbles than the control group, after 15 min and after 30 min.

4 Discussion

This study provides a comparative assessment of the neurotoxic potential of different nanoparticles, integrating histopathological, immunohistochemical, and behavioral endpoints. Our results consistently demonstrate that

Table 5 The hole-board test results

The hole-board test	Average time spent in thigmotaxis (min)	Average number of head-dipping	Average number of rearing	Average number of movements to the center	Stress index
Control	12.5 ± 1.9	7.6 ± 1.1	8.1 ± 1.2	6.6 ± 1.2	54.3 ± 8.1
SiO_2 NPs	8.8 ± 1.3	4.3 ± 0.8	3.9 ± 0.7*	2.8 ± 0.5*	80.0 ± 12.0*
NiO NPs	7.3 ± 1.6*	3.5 ± 0.5*	4.4 ± 0.7*	1.6 ± 0.6*	76.8 ± 12.5*
Co_3O_4 NPs	9.1 ± 2.1	3.4 ± 0.8*	2.8 ± 0.7*	3.7 ± 0.8*	91.9 ± 15.8*
Perovskite NPs	5.5 ± 0.8*	1.8 ± 0.6*	3.2 ± 0.5*	2.4 ± 0.5*	85.9 ± 13.9*
p-value	0.03	0.001	0.004	< 0.001	0.003
Size effect (η^2)	0.50	0.72	0.65	0.75	0.68

p value was calculated using one-way *ANOVA* test. "*" indicates statistical difference using post hoc Tukey test in comparison with the control group. η^2 indicates a large effect size

Table 6 The tail suspension test results

Tail suspension test	Mobility average times (s)	Immobility average time (s)	Average number of escapes	Average number of rests	Depression-like behavioral index
Control	397 ± 40	204 ± 20	24.2 ± 2.4	7.8 ± 1.2	30.8 ± 4.6
SiO_2 NPs	298 ± 52	301 ± 30*	19.7 ± 2.0	12.2 ± 1.9*	50.3 ± 12.5
NiO NPs	135 ± 19*	465 ± 47*	14.5 ± 3.5*	21.9 ± 5.3*	77.5 ± 11.6*
Co_3O_4 NPs	195 ± 27*	406 ± 41*	12.8 ± 2.3*	16.4 ± 4.5*	67.6 ± 16.1*
Perovskite NPs	169 ± 17*	431 ± 43*	9.8 ± 1.7*	14.3 ± 4.1*	71.8 ± 15.8*
p-value	0.01	< 0.001	0.02	0.009	0.02
Size effect (η^2)	0.62	0.85	0.58	0.63	0.60

p value was calculated using one-way *ANOVA* test. "*" indicates statistical difference using post hoc Tukey test in comparison with the control group. η^2 indicates a large effect size

Table 7 The forced swimming test results

Forced swimming test	Swimming time (s)	Immobility time (s)	Number of swimming	Average time spent in arrest	Number of climbing attempts	Depression index
Control	407 ± 31	193 ± 22	8.6 ± 1.0	5.7 ± 0.8	10.3 ± 1.3	32.2 ± 4.8
SiO_2 NPs	332 ± 39	267 ± 41*	7.5 ± 0.9	10.7 ± 2.3*	19.5 ± 2.9*	44.2 ± 5.6*
NiO NPs	181 ± 31*	419 ± 42*	14.5 ± 1.8*	21.5 ± 3.7*	25.3 ± 4.8*	69.8 ± 18.5*
Co_3O_4 NPs	221 ± 42*	379 ± 61*	8.6 ± 1.0	12.3 ± 2.9*	29.6 ± 6.4*	63.1 ± 12.5*
Perovskite NPs	171 ± 25*	428 ± 52*	4.7 ± 0.6*	17.1 ± 4.1*	13.6 ± 2.0*	71.3 ± 10.7*
p-value	0.01	0.007	0.04	< 0.001	0.003	0.01
Size effect (η^2)	0.61	0.67	0.53	0.80	0.70	0.62

p value was calculated using one-way *ANOVA* test. "*" indicates statistical difference using post hoc Tukey test in comparison with the control group. η^2 indicates a large effect size

perovskite NPs exerted the most pronounced neurotoxic effects, followed by Co_3O_4 NPs and NiO, while SiO_2 NPs induced relatively mild but still detectable alterations. The severity ranking was consistent across histopathology, nitrosative/oxidative stress, and neurobehavioral performance.

Regarding histopathological findings, there was a progressive loss of structural integrity, from mild changes with SiO_2 NPs to severe gliosis, neuronal degeneration, extensive vascular congestion, perivascular edema, neuropil vacuolation, spongiosis, and inflammatory infiltration with perovskite nanomembrane. According to the cumulative histopathology scores, perovskite

Table 8 The multiradial maze test results

Group	Average # of visited arms	Average # of entries into the arm with food	Average # of re-entries to arms with no food	Reference memory index	Working memory index
Control	11.3 ± 0.9	9.7 ± 1.2	3.6 ± 0.6	0.88 ± 0.07	3.6 ± 0.5
SiO_2 NPs	7.4 ± 1.2*	2.5 ± 0.4*	1.9 ± 0.7*	0.34 ± 0.08*	1.9 ± 0.5*
NiO NPs	8.2 ± 1.3*	3.1 ± 0.6*	2.1 ± 0.7*	0.39 ± 0.06*	2.1 ± 0.6*
Co_3O_4 NPs	6.8 ± 0.7*	2.4 ± 0.4*	1.7 ± 0.8*	0.35 ± 0.05*	1.7 ± 0.4*
Perovskite NPs	5.6 ± 0.8*	1.9 ± 0.8*	1.3 ± 0.4*	0.34 ± 0.05*	1.3 ± 0.3*
p-value	0.007	< 0.001	0.03	0.001	0.01
Size effect (η^2)	0.65	0.82	0.50	0.75	0.63

p value was calculated using one-way *ANOVA* test. "*" indicates statistical difference using post hoc Tukey test in comparison with the control group. η^2 indicates a large effect size

Table 9 Morris water-maze test results

Morris water-maze test	Average escape latency (s) (time to find the platform)	Average time spent in swimming (s)	Average time spent in immobility (s)	Average # of climbing attempts	Memory error index
Control	109 ± 11	92 ± 7	17 ± 2	14.8 ± 1.7	0.34 ± 0.05
SiO_2 NPs	156 ± 24*	122 ± 14	31 ± 4*	10.6 ± 1.5*	0.63 ± 0.08*
NiO NPs	127 ± 23	88 ± 5*	39 ± 5*	8.2 ± 1.2*	0.75 ± 0.09*
Co_3O_4 NPs	112 ± 19	69 ± 6*	41 ± 5*	5.2 ± 0.8*	0.96 ± 0.11*
Perovskite NPs	142 ± 21*	89 ± 4*	63 ± 7*	5.3 ± 1.2*	1.15 ± 0.13*
p-value	0.003	0.04	< 0.001	0.03	< 0.001
Size effect (η^2)	0.68	0.51	0.88	0.52	0.85

p value was calculated using one-way *ANOVA* test. "*" indicates statistical difference using post hoc Tukey test in comparison with the control group. η^2 indicates a large effect size

Table 10 Marble-burying test results in two rounds ($T = 15$, 30 min)

Marble-burying test (number of marbles = 20)	Average number of marbles buried after 15 min	Average number of marbles buried after 30 min	Compulsive–Obsessive Index (COI)
Control	6.45 ± 0.8	11.72 ± 1.5	1.10 ± 0.05
SiO_2 NPs	4.16 ± 0.8*	7.83 ± 1.1*	1.40 ± 0.11*
NiO NPs	3.28 ± 0.5*	4.67 ± 0.7*	1.60 ± 0.13*
Co_3O_4 NPs	1.8 ± 0.4*	2.57 ± 0.7*	1.78 ± 0.12*
Perovskite NPs	4.5 ± 0.6*	8.1 ± 1.9	1.37 ± 0.11
p-value	0.02	0.03	0.01
Size effect (η^2)	0.58	0.55	0.62

p value was calculated using one-way *ANOVA* test. "*" indicates statistical difference using post hoc Tukey test in comparison with the control group. η^2 indicates a large effect size

nanomembranes are the most harmful, followed by Co_3O_4 and NiO. These effects may be attributed to their heightened reactivity at the nanoscale, which enables their interactions with brain tissues components, triggering oxidative stress and inflammation, ultimately disrupting brain structure and function [33].

In the present study, silicon dioxide NPs have been associated with prominent gliosis and neuronophagia in agreement with Limón-Pacheco et al. [34]. These effects are likely mediated through oxidative stress and inflammation, which activate microglia and astrocytes, contributing to gliosis [35, 36]. Neuronophagia, clusters of

glial cells surrounding degenerating neurons, is a known response to primary neuronal injury [37]. The presence of shrunken, pyknotic neurons further suggests necrotic or apoptotic cell death, possibly driven by mitochondrial dysfunction [38]. Additionally, vascular congestion observed following NiO NPs exposure may indicate ROS-induced BBB compromise with resultant increased permeability and cerebral blood flow dysregulation, which may lead to ischemia, memory loss, and behavioral dysfunctions [39–41]. It has been reported that ROS-mediated apoptosis contributes to the neurodevelopmental and neurobehavioral effects associated with ambient NiO NPs [42]. The observations of the present study agree with Boukholda et al. [43], who demonstrated that subacute exposure to Co_3O_4 NPs leads to neuronal shrinkage and vacuolation in the cerebral cortex and striatum, along with cognitive deficits, anxiety, and depressive-like behaviors. These effects were attributed to oxidative stress and neuroinflammation. Perivascular edema likely results from BBB breakdown or vascular injury, while disrupted neuropil suggests extracellular matrix disorganization around neurons [44, 45]. Reactive gliosis and neuroinflammation were evident after exposure to perovskite nanomembrane, as indicated by glial proliferation. This response may reflect attempts to repair neuronal injury and contain ongoing damage [46, 47]. Neurotoxicity induced by these nanomaterials could be due to ROS generation associated with chronic exposure [48]. Neural spongiosis, indicated by neuronal swelling, suggests cytotoxic effects that disrupt brain homeostasis [49, 50]. Neuropil vacuolation may stem from synaptic degeneration linked to fluid accumulation from BBB disruption [51].

In this study, NPs-induced histopathological changes were accompanied by nitrosative and oxidative stress, evidenced by increased iNOS protein expression in NPs-treated groups. These findings highlight redox imbalance as a central mechanism of NPs neurotoxicity. Comparable effects have been reported for Co_3O_4 NPs, which elevate lipid peroxidation, protein oxidation, and nitrite levels while depleting antioxidant defenses, leading to cognitive deficits [43]. NiO NPs similarly induce ROS, upregulate iNOS, and increase lipid peroxidation, confirming their systemic and neural toxicity [52].

The iNOS induction promotes excess NO, which reacts with superoxide to form peroxynitrite, a potent oxidant that damages lipids, DNA, and proteins, driving cellular dysfunction [53]. The high oxidative/nitrosative burden and mitochondrial disruption observed with NiO, Co_3O_4, and perovskite NPs likely underpin the neurodegeneration noted in this study [54]. Progressive immunohistochemical changes were paralleled by behavioral alterations: Perovskite and NiO NPs groups showed pronounced anxiety and depression-like phenotypes in the raised plus-maze, forced swim, and tail suspension tests, while perovskite- and Co_3O_4-exposed mice displayed the most severe cognitive impairments in the multiradial and Morris water mazes. Co_3O_4 NPs further produced the strongest compulsive–obsessive tendencies, as reflected by the marble-burying test.

Co_3O_4 NPs in aged rats reinforce this pattern, increasing MDA, protein oxidation, and nitrite levels while reducing antioxidant defenses. These changes correlate with cognitive decline, anxiety and depression-like behaviors, and neuronal degeneration in the striatum and cerebral cortex [43]. NiO NPs exposure produces similar outcomes, with oxidative/nitrosative stress linked to histopathological alterations and liver toxicity [55].

Although in vivo data on perovskite nanomembranes in neural contexts are scarce, their strong effects in this study (highest histopathological scores, anxiety and depression indices, and memory errors) suggest high reactivity, ROS/RNS generation, brain penetration, and poor clearance may drive their toxicity. Supporting evidence shows lead bromide, a component of perovskite NPs, induces calcium overload, mitochondrial dysfunction, and apoptosis, impairing hippocampal learning and memory [56]. Lead halide perovskite quantum dots likewise reduce locomotor activity and elevate oxidative stress, underscoring their neurotoxic potential [57]. The findings of the present work may indicate that iNOS induction may be related to cellular stress and may explain stressful effect of the NPs exposure under study.

The variation in anxiety indices observed in the elevated plus-maze test may be due to oxidative stress and/or metal ion release from NPs, disrupting neurotransmitter homeostasis [58–61]. Changes in time spent in the closed arms reflect the anxiogenic potential of these NPs [62, 63]. Cognitive and exploratory deficits observed in the light–dark box test further support their neurotoxic impact [64]. Among all groups, cobalt oxide NPs-treated mice showed the highest anxiety index, likely due to neurotransmitter disruption and severe neurotoxicity [65]. Perovskite-treated mice also demonstrated elevated anxiety, potentially due to oxidative and functional neuronal damage [66].

Thigmotaxis, wall-hugging behavior was reduced in NPs-treated mice during the hole-board test, indicating altered anxiety or stress levels [67, 68]. Head-dipping, an exploratory behavior, was significantly diminished across NPs-treated groups, suggesting cognitive deficits and anxiety [69]. Perovskite-treated mice had the lowest head-dipping frequency, indicating severe neurotoxicity. Rearing behavior, indicative of vertical exploration and motor activity, was also reduced, reflecting lethargy or motor dysfunction [70]. These behavioral alterations

are consistent with glial and neuronal pathologies that impair cognition and increase anxiety [71].

Behavioral alterations seen in tail suspension test concerning mobility may be attributed to neurotoxicity as previously reported by Mishra [72]. Neurobehavioral disturbances may be associated with disrupt in mitochondrial function and neurotransmitter imbalance, as noted in earlier studies [73, 74]. Furthermore, perovskite nanomaterials, which contain lead, may interfere with neurochemical pathways and potentially cause behavioral deficits, as reported by Mukherjee et al. [75]. In addition, alterations in swimming and immobility times as seen in the forced swimming test may result from neurotoxicity induced by chronic exposure to NPs. This finding is consistent with prior studies reporting that NPs can trigger impacts on the central nervous system pointing to pronounced depressive-like behaviors and motor dysfunction [75]. Notably, NiO NPs and Co_3O_4 NPs have been linked to neurotoxicity through mechanisms such as oxidative stress, apoptosis, and disruptions in dopaminergic or adrenergic signaling pathways [76]. However, perovskite nanomembrane caused significant behavioral impairments, potentially due to neurotoxicity associated with mitochondrial dysfunction, and disruption of neuronal signaling pathways [77]. However, all NPs-treated mice under study demonstrated an elevation in the depression index compared to control ones, with perovskite-treated mice showed the most pronounced effect. These findings align with the previous studies highlighting the potential of NPs to induce neurobehavioral deficits caused by neurochemical imbalances [78].

The multiradial maze test demonstrated marked reductions in reference and working memory indices in NPs-treated groups, especially in perovskite-treated mice. These results suggest significant cognitive impairment due to long-term NPs exposure. The hippocampus, particularly the dentate gyrus and CA subfields, is crucial for spatial navigation and memory consolidation. Damage to these areas can lead to disorientation, memory loss, and cognitive deficits [79–82].

The findings of Morris maze test were consistent with and corroborated the results of the above-mentioned neurobehavioral findings. Exposure to NPs understudy indicates neurotoxicity as reflected by increased escape latency and reduced spatial learning performance [83]. These behavioral deficits might be resulted from reduced motivation, neuromuscular impairment, or cognitive dysfunction [84, 85]. Overall, these results suggest that exposure to NPs compromises spatial learning and memory, with effects likely modulated by particle size, chemical composition, and bioavailability [86, 87]. Perovskites, due to their lead content, may cause more severe oxidative and neurotoxic damage [14].

In the marble-burying test, the Compulsive–Obsessive Index (COI) was significantly altered across all NPs-treated groups when compared to controls, indicating varying degrees of neurobehavioral disruption. Mice treated with SiO_2 NPs and perovskite nanomembranes demonstrated moderately elevated COI values suggesting the presence of anxiety- or compulsive-like behavior, potentially mediated by oxidative stress and its influence on underlying neurochemical pathways [88]. In contrast, mice subjected to Co_3O_4 and NiO NPs exhibited high COI indicating significant neurobehavioral toxicity, possibly due to profound neurotransmitter dysregulation or oxidative damage indicating disruption in dopamine signaling [89, 90].

5 Conclusions

The present study demonstrates that chronic exposure to the tested NPs leads to significant histological and behavioral neurotoxicity. Brain regions such as the cerebral cortex, hippocampal subfields, particularly the dentate gyrus and cerebellar cortex exhibited signs of pyknotic neurons, vascular congestion, gliosis, and perivascular edema, indicative of oxidative stress, inflammation, and irreversible neuronal damage. Neurobehavioral assessments revealed heightened anxiety, depression, and stress responses, along with impaired memory, reduced motor activity, and compulsive behaviors, with both reference and working memory significantly affected. Among the tested NPs, perovskite nanomembranes induced the most severe effects, followed by Co_3O_4, NiO, and SiO_2 NPs. These findings underscore the neurotoxic potential of various NPs and emphasize the urgent need for thorough safety evaluations prior to their use in medical, environmental, or industrial applications. Future research should prioritize long-term studies aimed at uncovering the precise molecular mechanisms behind these toxic effects and their broader physiological implications.

5.1 Limitations

Although intraperitoneal administration ensures consistent systemic exposure, it does not replicate common human exposure routes such as oral, inhalation, or dermal pathways. This limits the translational relevance of the findings. Future studies should incorporate more environmentally and physiologically relevant exposure methods to better reflect human risk and to complement the mechanistic insights provided by the current IP model.

In addition, the present work was conducted exclusively in male BALB/c mice. Given the well-documented

sex differences in neurobehavioral responses, the exclusion of female cohorts restricts the generalizability of the results. Future research should include both sexes to determine whether the observed effects are consistent across genders.

Furthermore, while a comprehensive battery of neurobehavioral tests was employed, the potential for stress-related carry-over effects between tasks cannot be entirely ruled out. Randomization and counterbalancing of the test sequence were implemented to mitigate this risk, and these measures were considered appropriate given the sample size ($n=10$). Nevertheless, residual carry-over effects remain a possible limitation. Future studies could address this by increasing group sizes, optimizing the sequencing of behavioral tasks, or incorporating longer recovery intervals between tests.

Abbreviations

BBB	Blood–Brain Barrier
CA	Cornu Ammonis
CAS	Chemical abstracts service
COI	Compulsive–obsessive index
FTIR	Fourier transform infrared
H&E	Hematoxylin and eosin
IP	Intraperitoneal
NPs	Nanoparticles
RMI	Reference memory index
RNS	Reactive nitrogen species
ROS	Reactive oxygen species

Acknowledgements
This work was supported by the Researchers Supporting Project (ORF-2025-900) at King Saud University, Riyadh, Saudi Arabia. The authors would also like to express their gratitude to the Deanship of Scientific Research at King Khalid University, Abha, Saudi Arabia, for supporting this research through grant number RGP2/178/46. Additionally, the authors sincerely thank Jerash University for providing access to their laboratory facilities. In addition, the authors acknowledge the support of Isra University, Jordan, in accordance with the decision of the Deans' Council (No. 2025/2024/11-42), for facilitating this research participation.

Author contribution
B.J. was responsible for project administration, research preformation, conceptualization, supervision and validation, and writing the original draft; M.A. contributed to conceptualization, methodology, resources, funding acquisition, and writing the original draft; A.A. performed conceptualization, validation, investigation, methodology, and formal analysis; Q.J. participated in investigation, supervision, data curation, and resource management; S.L. was involved in conceptualization, data analysis, writing, review, and editing the manuscript; E.S.Z. contributed to conceptualization, writing—review and editing, data curation, and data analysis; and A.S. has contributed to project administration, methodology, investigation, and supervision, and writing, review, and editing the manuscript. All authors read and approved the final manuscript.

Funding
This study was funded by the Researchers Supporting Project (ORF-2025-900) at King Saud University, Riyadh, Saudi Arabia, the Deanship of Scientific Research at King Khalid University, Abha, Saudi Arabia, Grant Number (RGP2/178/46).

Data availability
The raw data supporting the present study will be made available by the corresponding author upon request, without undue reservation.

Declarations

Ethic statement
All experimental procedures conducted in the present study were approved by the Ethics Committee of Jerash University (Approval No. 3/6/2024/2025).

Competing interests
The authors declare no competing interests.

Author details
[1]Jerash University, Jerash, Jordan. [2]King Saud University, Riyadh, Saudi Arabia. [3]King Khalid University, Abhā, Saudi Arabia. [4]Isra University, Amman, Jordan. [5]Universiti Putra Malaysia, Seri Kembangan, Malaysia. [6]Inje University, Gimhae, Republic of Korea. [7]Zagazig University, Zagazig, Egypt.

Received: 27 March 2025 Accepted: 28 September 2025
Published online: 09 October 2025

References

1. Malik S, Muhammad K, Waheed Y (2023) Emerging applications of nanotechnology in healthcare and medicine. Molecules 18:6624
2. Gao X, Cui Y, Levenson RM, Chung LW, Nie S (2004) In vivo cancer targeting and imaging with semiconductor quantum dots. Nat Biotechnol 22(8):969–976. https://doi.org/10.1038/nbt994
3. Alagar V, Kumar S, Rajasekaran KM (2015) Nanoparticles in catalysis: opportunities and challenges. J Nanosci Nanotechnol 15(1):39–59
4. Patil VS, Patil A, Patil R (2018) Nanotechnology in agriculture: scope and constraints. Appl Mater Today 10:155–172
5. Suvarna V, Nair A, Mallya R, Khan T, Omri A (2022) Antimicrobial nanomaterials for food packaging. Antibiotics 11(6):729. https://doi.org/10.3390/antibiotics11060729
6. Gupta V et al (2022) Nanotechnology in cosmetics and cosmeceuticals-a review of latest advancements. Gels 8(3):173
7. Dastgeer G, Nisar S, Zulfiqar M, Eom J, Imran M, Kamran K (2024) A review on recent progress and challenges in high-efficiency perovskite solar cells. Nano Energy 132:110401. https://doi.org/10.1016/j.nanoen.2024.110401
8. Almansour M, Alarifi S, Jarrar B (2018) In vivo investigation on the chronic hepatotoxicity induced by intraperitoneal administration of 10 nm silicon dioxide nanoparticles. Int J Nanomed 13:2685–2996
9. Tiedemann D et al (2017) Toxicity of cobalt oxide nanoparticles in human and rodent models. NanoImpact 6:34–41
10. Jarrar B, Almansour M, Jarrar Q, Al-Doaiss A, Lee SY, Boudemagh D (2024) Toxicity assessment of copper oxide nanoparticles: *in vivo* study. Nanotechnol Rev 13(1):20240122. https://doi.org/10.1515/ntrev-2024-0122
11. Jarrar B, Al-Doaiss A, Shati A, Al-Kahtani M, Jarrar Q (2021) Behavioural alterations induced by chronic exposure to 10 nm silicon dioxide nanoparticles. IET Nanobiotechnol 15(2):221–235. https://doi.org/10.1049/nbt2.12041
12. Abouzeinab NS, Kahil N, Fakhruddin N, Awad R, Khalil MI (2023) Intraperitoneal hepato-renal toxicity of zinc oxide and nickel oxide nanoparticles in male rats: biochemical, hematological and histopathological studies. EXCLI J 22:619–644. https://doi.org/10.17179/excli2023-6237
13. Li J, Wang J, Wang YL, Luo Z, Zheng C, Yu G, Wu S, Zheng F, Li H (2021) Nox2 activation contributes to cobalt nanoparticles-induced inflammatory responses and Tau phosphorylation in mice and microglia. Ecotoxicol Environ Saf 225:112725. https://doi.org/10.1016/j.ecoenv.2021.112725
14. Makableh Y, Jarrar B, Al-Shdaifat A (2024) Toxicity assessment of perovskite nanocomposites: in vivo study. Toxicol Ind Health 40(3):75–90. https://doi.org/10.1177/07482337231224512
15. Jarrar B, Taib N (2018) Histocytotechnology, 3rd edn. King Saud University Press, Riyadh
16. Hasturk AE, Yilmaz ER, Turkoglu E, Kertmen H, Horasanli B, Hayirli N, Erguder IB, Evirgen O (2015) Therapeutic evaluation of interleukin 1-beta antagonist Anakinra against traumatic brain injury in rats. Ulus Travma Acil Cerrahi Derg 21(1):1–8. https://doi.org/10.5505/tjtes.2015.57894
17. Arac D, Erdi MF, Keskin F, Kenan M, Cuce G, Aydemir FHY, Guney O, Kocaogullar Y (2021) Neuroprotective effects of milrinone on

experimental acute spinal cord injury: rat model. World Neurosurg 147:e225–e233. https://doi.org/10.1016/j.wneu.2020.12.021

18. Torlakovic EE, Nielsen S, Vyberg M, Taylor CR (2015) Getting controls under control: the time is now for immunohistochemistry. J Clin Pathol 68:879–882. https://doi.org/10.1136/jclinpath-2014-202705
19. Sewelam A, Kabil LS, Jarrar MB, Sabry M, Morsy M (2024) *Lycium barbarum* polysaccharide attenuates acute toxicity caused by titanium dioxide nanoparticles in splenic and pulmonary tissues. Pharm Sci 30(3):339–354. https://doi.org/10.34172/PS.2024.15
20. Walf A, Frye C (2007) The use of the elevated plus maze as an assay of anxiety-related behavior in rodents. Nat Protoc 2:322–328. https://doi.org/10.1038/nprot.2007.44
21. Kraeuter AK, Guest PC, Sarnyai Z (2019) The elevated plus maze test for measuring anxiety-like behavior in rodents. Methods Mol Biol 1916:69–74. https://doi.org/10.1007/978-1-4939-8994-2_4
22. Arrant AE, Schramm-Sapyta NL, Kuhn CM (2013) Use of the light/dark test for anxiety in adult and adolescent male rats. Behav Brain Res 256:119–127
23. Bourin M, Hascoët M (2003) The mouse light/dark box test. Eur J Pharmacol 463(1–3):55–65. https://doi.org/10.1016/s0014-2999(03)01274-3
24. Brown GR, Nemes C (2008) The exploratory behaviour of rats in the hole-board apparatus: is head-dipping a valid measure of neophilia? Behav Processes 78(3):442–448. https://doi.org/10.1016/j.beproc.2008.02.019
25. Can A, Dao DT, Terrillion CE, Piantadosi SC, Bhat S, Gould TD (2012) The tail suspension test. J Vis Exp 59:e3769. https://doi.org/10.3791/3769
26. Yankelevitch-Yahav R, Franko M, Huly A, Doron R (2015) The forced swim test as a model of depressive-like behavior. J Vis Exp 97:52587. https://doi.org/10.3791/52587
27. Can A, Dao DT, Arad M, Terrillion CE, Piantadosi SC, Gould TD (2012) The mouse forced swim test. J Vis Exp 59:e3638. https://doi.org/10.3791/3638
28. Samuelson EE, Chen-Wishart ZP, Gill RJ, Leadbeater E (2016) Effect of acute pesticide exposure on bee spatial working memory using an analogue of the radial-arm maze. Sci Rep 6:38957
29. Vorhees CV, Williams MT (2014) Assessing spatial learning and memory in rodents. ILAR 55(2):310–332. https://doi.org/10.1093/ilar/ilu013
30. Vorhees CV, Williams MT (2006) Morris water maze: procedures for assessing spatial and related forms of learning and memory. Nat Protoc 1(2):848–858. https://doi.org/10.1038/nprot.2006.116
31. de Brouwer G, Fick A, Harvey BH, Wolmarans W (2019) A critical inquiry into marble-burying as a preclinical screening paradigm of relevance for anxiety and obsessive-compulsive disorder: mapping the way forward. Cogn Affect Behav Neurosci 19(1):1–39. https://doi.org/10.3758/s13415-018-00653-4
32. Angoa-Pérez M, Kane MJ, Briggs DI, Francescutti DM, Kuhn DM (2013) Marble burying and Nestlet shredding as tests of repetitive, compulsive-like behaviors in mice. J Vis Exp 82:50978. https://doi.org/10.3791/50978
33. Karmakar A, Zhang Q, Zhang Y (2014) Neurotoxicity of nanoscale materials. J Food Drug Anal 22(1):147–160. https://doi.org/10.1016/j.jfda.2014.01.012
34. Limón-Pacheco JH, Jiménez-Barrios N, Déciga-Alcaraz A, Martínez-Cuazitl A, Mata-Miranda MM, Vázquez-Zapién GJ, Pedraza-Chaverri J, Chirino YI, Orozco-Ibarra M (2020) Astrocytes are more vulnerable than neurons to silicon dioxide nanoparticle toxicity in vitro. Toxics 8(3):51. https://doi.org/10.3390/toxics8030051
35. Wei W, Sun H, Yang B, Song E, Song Y, Apo E (2024) Protein combines with LRP1 to inactivate GSK3β that mitigates silica nanoparticle-induced brain lesion. ACS Chem Neurosci 15(4):808–815
36. Hou S, Li C, Wang Y, Sun J, Guo Y, Ning X, Ma K, Li X, Shao H, Cui G, Jin M, Du Z (2022) Silica nanoparticles cause activation of NLRP3 inflammasome in-vitro model-using microglia. Int J Nanomed 17:5247–5264. https://doi.org/10.2147/IJN.S372485
37. Wang R, Zhou R, Chen Z, Gao S, Zhou F (2022) The glial cells respond to spinal cord injury. Front Neurol 13:844497. https://doi.org/10.3389/fneur.2022.844497
38. Poupot R, Bergozza D, Fruchon S (2018) Nanoparticle-based strategies to treat neuro-inflammation. Materials 11(2):270. https://doi.org/10.3390/ma11020270
39. Mauricio MD, Guerra-Ojeda S, Marchio P, Valles SL, Aldasoro M, Escribano-Lopez I, Herance JR, Rocha M, Vila JM, Victor VM (2018) Nanoparticles in medicine: a focus on vascular oxidative stress. Oxid Med Cell Longev 2018:6231482. https://doi.org/10.1155/2018/6231482
40. Chen T, Dai Y, Hu C, Lin Z, Wang S, Yang J, Zeng L, Li S, Li W (2024) Cellular and molecular mechanisms of the blood-brain barrier dysfunction in neurodegenerative diseases. Fluids Barriers CNS 21(1):60. https://doi.org/10.1186/s12987-024-00557-1
41. Han HY (2022) Sublethal pulmonary toxicity screening of silica nanoparticles in rats after direct intratracheal instillation. Toxicol Res 38:523–530
42. Wang Z, Bi Y, Li K, Song Z, Pan C, Zhang S, Lan X, Foulkes NS, Zhao H (2023) Nickel oxide nanoparticles induce developmental neurotoxicity in zebrafish by triggering both apoptosis and ferroptosis. Environ Sci Nano 10(2):640–655
43. Boukholda K, Elwej A, Abdelkodous M, Ammar R, Slimen SB, Fiebich BL, Bouchard M, Fetoui H, Chtourou Y (2025) Toxicological alterations induced by subacute exposure of cobalt oxide nanoparticles in aged rats: behavioral, biochemical, molecular, and histopathological evidence. Biol Trace Elem Res Mar 8:1–13
44. Solar P, Hendrych M, Barak M, Valekova H, Hermanova M, Jancalek R (2022) Blood-brain barrier alterations and edema formation in different brain mass lesions. Front Cell Neurosci 16:922181. https://doi.org/10.3389/fncel.2022.922181
45. Syková E, Voříšek I, Starčuk Z, Kratochvíla J, Pavlova I, Ichikawa Y, Kwok JCF, Kmoníčková E, Myronchenko S, Hromádka T, Smolek T, Avila M, Basheer N, Žilka N (2025) Disruption of extracellular matrix and perineuronal nets modulates extracellular space volume and geometry. J Neurosci 45(8):e0517242024. https://doi.org/10.1523/JNEUROSCI.0517-24.2024
46. Barres BA (2008) The mystery and magic of glia: a perspective on their roles in health and disease. Neuron 60(3):430–440
47. Virtuoso A, De Luca C, Korai SA, Papa M, Cirillo G (2023) Neuroinflammation and glial activation in the central nervous system: a metabolic perspective. Neural Regen Res 18(5):1025–1026. https://doi.org/10.4103/1673-5374.355754
48. García MA et al (2021) Nanotoxicology: a comprehensive review of the mechanisms of nanomaterial-induced toxicity. Nanotoxicol 15(1):1–30
49. Riediker M et al (2019) Particle toxicology and health-where are we? Part Fibre Toxicol 16(1):1–30. https://doi.org/10.1186/s12989-019-0302-8
50. Trbojevich RA, Khare S, Lim JH, Watanabe F, Gokulan K, Krohmaly K, Williams K (2020) Assessment of silver release and biocidal capacity from silver nanocomposite food packaging materials. Food Chem Toxicol 145:111728. https://doi.org/10.1016/j.fct.2020.111728
51. Pujalté I, Dieme D, Haddad S, Serventi AM, Bouchard M (2016) Toxicokinetics of titanium dioxide (TiO_2) nanoparticles after inhalation in rats. Toxicol Lett 265:1–8
52. Siddiqui MA, Ahamed M, Ahmad J, Majeed Khan MA, Musarrat J, Al-Khedhairy AA, Alrokayan SA (2012) Nickel oxide nanoparticles induce cytotoxicity, oxidative stress and apoptosis in cultured human cells that is abrogated by the dietary antioxidant curcumin. Food Chem Toxicol 50(3–4):641–647. https://doi.org/10.1016/j.fct.2012.01.017
53. Jomova K, Raptova R, Alomar SY, Alwasel SH, Nepovimova E, Kuca K, Valko M (2023) Reactive oxygen species, toxicity, oxidative stress, and antioxidants: chronic diseases and aging. Arch Toxicol 97(10):2499–2574. https://doi.org/10.1007/s00204-023-03562-9
54. Selvaraj NR, Nandan D, Nair BG, Nair VA, Venugopal P, Aradhya R (2025) Oxidative stress and redox imbalance: common mechanisms in cancer stem cells and neurodegenerative diseases. Cells 14(7):511. https://doi.org/10.3390/cells14070511
55. Yu S, Liu F, Wang C, Zhang J, Zhu A, Zou L, Han A, Li J, Chang X, Sun Y (2018) Role of oxidative stress in liver toxicity induced by nickel oxide nanoparticles in rats. Mol Med Rep 17(2):3133–3139
56. Linqiang M et al (2023) Neurotoxicity study of lead-based perovskite nanoparticles. Nano Today 50:101830. https://doi.org/10.1016/j.nantod.2023.101830
57. Ngo LT et al (2023) Comprehensive neurotoxicity of lead halide perovskite nanocrystals in nematode *Caenorhabditis elegans*. Small 20(2):e2306020. https://doi.org/10.1002/smll.202306020
58. Al-Ruwaili M, Jarrar B, Jarrar Q, Al-Doaiss A, Alshehri M, Melhem W (2022) Renal ultrastructural damage induced by chronic exposure to copper oxide nanomaterials: electron microscopy study. Toxicol Ind Health 38(2):80–91. https://doi.org/10.1177/07482337211062674
59. Sagadevan S, Fatimah I, Anita L, Jayasingh R, Zillur Leonard E, Won-Chun O (2023) Eco-friendly green approach of nickel oxide nanoparticles for biomedical applications. Open Chem 21(1):20230141. https://doi.org/10.1515/chem-2023-0141

60. Sharma P et al (2021) Neurobehavioral effects of nanoparticles: an overview of mechanisms and assessment methods. Environ Res 195:110835
61. Serra M, Simola N, Pollack AE, Costa G (2024) Brain dysfunctions and neurotoxicity induced by psychostimulants in experimental models and humans: an overview of recent findings. Neural Regen Res 1(9):1908–1918. https://doi.org/10.4103/1673-5374.390971
62. Korde V, Khot S, Kamble D, Amalraj S (2024) Review: Perovskite nanostructures materials versatile platform for advance biosensor applications. Sens Actuators Rep 7:100201. https://doi.org/10.1016/j.snr.2024.100201
63. Gong K, Yin X, Lu J, Zheng H, Wu W (2024) Silicon dioxide nanoparticles induce anxiety-like behavior in a size-specific manner via the microbiota-gut-brain axis. Environ Toxicol Pharmacol 109:104493. https://doi.org/10.1016/j.etap.2024.104493
64. Zhang Q, Ma X, Hou C (2019) Neurobehavioral impairments induced by nickel oxide nanoparticles. J Nanotoxicol 13(5):411–423
65. Ahmed S, Anwar F, Sherwani SK (2020) Effects of cobalt nanoparticles on neural and behavioral responses. Toxicol Rep 7:65–75
66. Huang X, Jiang J, Gao M (2022) Neurological impacts of perovskite nanomaterials: a review. Mater Today 45:21–35
67. Brown RE, Corey SC, Moore AK (1999) Differences in exploratory behavior in the elevated plus-maze and hole-board tests: implications for rodent models of anxiety. Behav Brain Res 101(1):103–112
68. Treit D, Fundytus M (1988) Thigmotaxis as a test for anxiolytic activity in rats. Pharmacol Biochem Behav 4:959–962
69. Takeda H, Tsuji M, Matsumiya T (1998) Changes in head-dipping behavior in the hole-board test reflect the anxiogenic and/or anxiolytic state in mice. Eur J Pharmacol 350(1):21–29
70. Heinz DE et al (2021) Exploratory drive, fear, and anxiety are dissociable and independent components in foraging mice. Transl Psychiatry 11:318. https://doi.org/10.1038/s41398-021-01458-9
71. Pentkowski NS, Rogge-Obando KK, Donaldson TN, Bouquin SJ, Clark BJ (2021) Anxiety and Alzheimer's disease: behavioral analysis and neural basis in rodent models of Alzheimer's-related neuropathology. Neurosci Biobehav Rev 127:647–658. https://doi.org/10.1016/j.neubiorev.05.005
72. Mishra D (2023) Biomedical applications of perovskite-based materials. In: Moharana S, Badapanda T, Satpathy SK, Mahaling RN, Kumar R (eds) Metal oxides, perovskite metal oxides. Elsevier, Amsterdam, pp 367–393. ISBN 9780323995290, https://doi.org/10.1016/B978-0-323-99529-0.00011-4.
73. Chen R, Yin J, Tang M (2016) Effects of nickel oxide nanoparticles on rat behavior and the potential neurotoxicity mechanisms. NanoImpact 3–4:91–97
74. Zhao F, Li J, Guan Y (2019) Neurotoxicity of cobalt nanoparticles and its mechanisms. Toxicol 415:1–10
75. Mukherjee S, Acharya S, Biswas D (2021) Toxicological insights into perovskite nanomaterials: mechanisms and implications. Nat Rev Mater 6(3):215–230
76. Zheng F, Luo Z, Zheng C, Li J, Zeng J, Yang H, Chen J, Jin Y, Aschner M, Wu S, Zhang Q (2019) Comparison of the neurotoxicity associated with cobalt nanoparticles and cobalt chloride in Wistar rats. Toxicol Appl Pharmacol 369:90–99. https://doi.org/10.1016/j.taap.2019.03.003
77. Murugadoss S, Lison D, Godderis L, Van Den Brule S, Mast J, Brassinne F, Sebaihi N, Hoet PH (2017) Toxicology of silica nanoparticles: an update. Arch Toxicol 91(9):2967–3010. https://doi.org/10.1007/s00204-017-1993-y
78. Gong JY, Holt MG, Hoet PHM, Ghosh M (2022) Neurotoxicity of four frequently used nanoparticles: a systematic review to reveal the missing data. Arch Toxicol 96(5):1141–1212. https://doi.org/10.1007/s00204-022-03233-1
79. Win-Shwe TT, Fujimaki H (2011) Nanoparticles and neurotoxicity. Int J Mol Sci 12(9):6267–6280
80. Zhu FD (2021) Nanoparticles: a hope for the treatment of inflammation in CNS. Front Pharmacol 12:683935
81. Teleanu DM, Chircov C, Grumezescu AM, Volceanov A, Teleanu RI (2018) Impact of nanoparticles on brain health: an up to date overview. J Clin Med 7(12):490
82. Bird C, Burgess N (2008) The hippocampus and memory: insights from spatial processing. Nat Rev Neurosci 9:182–194
83. You R, Ho YS, Hung CH, Liu Y, Huang CX, Chan HN, Ho SL, Lui SY, Li HW, Chang RC (2018) Silica nanoparticles induce neurodegeneration-like changes in behavior, neuropathology, and affect synapse through MAPK activation. Part Fibre Toxicol 15(1):28. https://doi.org/10.1186/s12989-018-0263-3
84. Hussain SM, Hess KL, Gearhart JM, Geiss KT, Schlager JJ (2005) In vitro toxicity of nanoparticles in BRL 3A rat liver cells. Toxicol In Vitro 7:975–983. https://doi.org/10.1016/j.tiv.2005.06.034
85. Ge D, Du Q, Ran B, Liu X, Wang X, Ma X, Cheng F, Sun B (2019) The neurotoxicity induced by engineered nanomaterials. Int J Nanomed 14:4167–4186. https://doi.org/10.2147/IJN.S203352
86. Gambini J, Stromsnes K (2022) Oxidative stress and inflammation: from mechanisms to therapeutic approaches. Biomedicines 10(4):753. https://doi.org/10.3390/biomedicines10040753
87. Chiang MC, Yang YP, Nicol CJB, Wang CJ (2024) Gold nanoparticles in neurological diseases: a review of neuroprotection. Int J Mol Sci 25(4):2360. https://doi.org/10.3390/ijms25042360
88. Adams TG, Kelmendi B, Brake CA, Gruner P, Badour CL, Pittenger C (2018) The role of stress in the pathogenesis and maintenance of obsessive-compulsive disorder. Chronic Stress 2:2470547018758043. https://doi.org/10.1177/2470547018758043
89. Hussain MF, Naeem Ashiq M, Gulsher M, Akbar A, Iqbal F (2020) Exposure to variable doses of nickel oxide nanoparticles disturbs serum biochemical parameters and oxidative stress biomarkers from vital organs of albino mice in a sex-specific manner. Biomarkers 25(8):719–724. https://doi.org/10.1080/1354750X.2020.1841829
90. Song B, Zhang Y, Liu J, Feng X, Zhou T, Shao L (2016) Is neurotoxicity of metallic nanoparticles the cascades of oxidative stress? Nanoscale Res Lett 11(1):291. https://doi.org/10.1186/s11671-016-1508-4

Publisher's Note